G2 Group Report

Virtual Wind Tunnel

2014

Supervisor: Dr Gavin Tabor

Luke Blades, Heather Bolt, Felix Browne, Edward Crinion, David Docherty, Luke Hamilton, Dan Nima, James Walton

Abstract

Wind tunnels are the industry standard technique for modelling aerodynamic flows around automotive designs. This project set out to investigate the integration of Computer Aided Design (CAD), Computational Fluid Dynamics (CFD) and experimental testing from an automotive design perspective. Traditionally, scale models of cars for testing purposes are handmade from clay and Additive Layer Manufacturing (ALM) has the potential to automate this manufacturing process and in turn decrease project lead times. The incorporation of this technique was investigated within the Virtual Wind Tunnel (VWT) project. The group was split into three sub-groups: Automotive Design, High Performance Computing (HPC) and Experimental Testing. The Design Group designed the concept car, identified optimum import and meshing strategies for CFD modelling, produced physical scale models and explored virtual rendering of the vehicle. The HPC Group examined different meshing techniques and turbulence models to develop a VWT for the concept car. Additionally, the velocity flow profiles for an urban environment were investigated and a surrogate-based modelling approach was explored. The Experimental Group designed and manufactured a new test section for one of the University of Exeter's wind tunnels and tested the concept car scale models to validate the VWT.

The final concept car from the Design Group was tested in the wind tunnel test section modified by the Experimental Group. The drag was measured using a drag balance which gave drag coefficients of 0.17 ± 0.015. A velocity wake survey was also conducted for the car at an angle of 14° off-centre; this was used to calculate a drag coefficient of 0.358 using Von Karman's integral formulation. The concept car was tested in the VWT under similar conditions to both experiments giving drag coefficients of 0.167 for head-on and 0.298 for the angled case.

Keywords:
Wind Tunnel, Drag Coefficient, CFD, Meshing, Automotive Design

The group would like to extend their gratitude to Dr. Gavin Tabor for his support and supervision.

Contents

1 Introduction

The aerodynamic properties of cars have a direct effect on their performance (fuel efficiency, stability, cooling etc.). To understand the aerodynamics and optimise their designs, automotive manufacturers test their cars in wind tunnels. Wind tunnels are typically used to replicate the conditions of a car moving through still air as closely as possible; this is done by moving air across a stationary model car. The aerodynamic properties of a car are inferred by measuring aspects of the flow around it.

Another method of examining fluid flow is to use computational fluid dynamics (CFD) to analyse fluid flows virtually. Time and money can be saved in a vehicle's development if its aerodynamic properties are tested virtually, parallel to physical wind tunnel tests. This report describes an investigation into how various aspects of aerodynamic evaluation are combined; including Computer Aided Design (CAD), CFD, scale model manufacture and physical testing. The project investigates how these aspects link together and explores the advantages of a mixed computational and practical approach to car design.

The overall project team was split into three sub-groups; a design group, a high performance computing group (HPC) and an experimental group. The design group was responsible for designing a concept car for the purposes of testing computationally and practically. The computational analysis would be performed by the HPC group by creating a virtual wind tunnel using CFD. The results of the CFD analysis would be compared to physical wind tunnel testing performed by the experimental group.

This report is an executive summary of the work carried out for this group project. For complete accounts of individual work packages which will be directly referred to throughout this report, see: Blades [1], Bolt[2], Browne [3], Crinion [4], Docherty [5], Hamilton [6], Nima [7], Walton [8]. This report firstly presents some relevant background information. It then goes on to describe how the project was undertaken, this methodology section explains how the final results were obtained. Results and analysis are then presented. Details of how the project was managed are then given, before the sustainability of the project is discussed.

1.1 Project Objectives and Deliverables

1.1.1 Project Objectives

This project had three primary objectives. Firstly, to investigate the integrated design approach to design the external body of a concept car using CAD, CFD and wind tunnel testing. Secondly, to explore the use of high performance computing (HPC) to create a virtual wind tunnel that would accurately simulate experimental results. Finally, to redesign the University's current wind tunnel facilities and use them to obtain experimental results to validate the VWT.

1.1.2 Project Deliverables

- To iteratively design a concept car using CAD and CFD.
- Virtually render the concept car using Blender.
- Design and build a new test chamber for the fluids laboratory wind tunnel, suitable for experimental testing of scaled car prototypes produced through Additive Layer Manufacture (ALM).
- Use the Ahmed body experimental results to create a virtual environment using CFD, to model aerodynamic flow behaviour.
- Import Ahmed body and concept car models into Ansys Fluent [9], Pointwise [10] and OpenFOAM [11] to compare and optimise meshing methods.
- Test concept car within VWT and compare with experimental results.

- Create velocity profiles for an urban environment and compare against classic wind tunnel flow profiles.
- Produce a surrogate model for the Ahmed body to investigate the use of this modelling technique in automotive design.

2 Background and Review of Existing Work

2.1 Wind Tunnel Operation

The aerodynamic properties of a vehicle are a product of the relative motion between it and the air around it. Therefore the aerodynamics of a car moving through still air are equivalent to air moving over a stationary car. Wind tunnels are typically used to replicate this as closely as possible. They are formed of four basic components; the effuser, the working section, the diffuser and the driving unit.

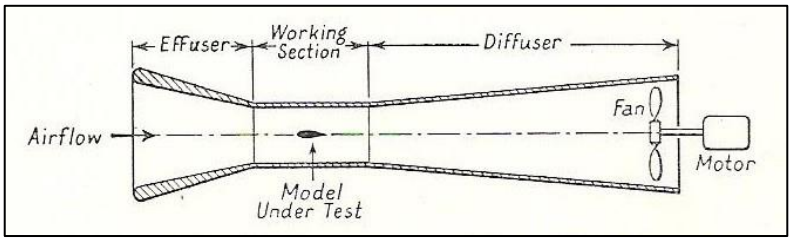

Figure 2-1 The locations of the four basic components of a wind tunnel [12]

These four components are shown in the diagram of an open circuit wind tunnel in Figure 2-1. The driving unit is typically a fan used to generate a continuous flow through the wind tunnel. The effuser is upstream of the test model, this is where the air is accelerated from rest to the inlet conditions at the start of the working section. The working section (also known as the test section) is where the testing takes place, the car model is placed here and measurements are taken. The diffuser sits downstream of the test section and is shaped to convert some of the kinetic energy of the flow at the exit of the test section into pressure energy to reduce the energy needed to keep the flow continuous.

Various types of measurement can be taken within the test section to determine the aerodynamic properties and forces on the model. Drag forces can be measured by placing the model on a drag balance or by measuring the velocities of the wake and determining how much momentum was lost. Air velocity is typically measured using pitot-tubes or hot-wire anemometers. The properties of the flow can also be seen visually by introducing smoke or particles into the flow.

2.2 Computational Fluid Dynamics (CFD)

Computational Fluid Dynamics (CFD) is a branch of fluid mechanics that uses computer simulations to analyse the flow of fluids in systems as well other fluid behaviours such as heat transfer and chemical reactions [13]. CFD is based upon the governing equations of fluid flow which are partial differential equations derived from the conservation laws of physics. The governing equations describe the conservation of mass, momentum and energy [14].

The complexity of these governing equations means that finding analytical solutions is often impossible for practical applications [15]. In order to solve practical fluid dynamics problems, the partial differential equations are discretised into a set of algebraic equations which can then be solved numerically [16]. The geometry of a given fluid flow problem, referred to from now on as the ‘domain’, is divided into many small volumes or ‘cells’, each perfectly contacting the face of adjacent volumes. The discretised algebraic equations are solved by

using the output of one cell as the input to another adjacent cell; this is done across the whole domain in order to calculate the properties of the fluid at each cell centre at discrete times and thus generate a CFD solution. In order to begin solving the equations it is necessary to provide an input to the problem; this is done by specifying 'boundary conditions' which describe the behaviour of the fluid at the outermost cell faces of the domain [16].

2.2.1 Mesh Generation

The creation of a mesh is a critical process within any CFD simulation, as it is this structure that allows the discretised versions of the fluid transport equations to be applied to a given flow. In order to predict macro-scale fluid behaviour, fluxes - such as momentum - are considered to be constant over each cell within a mesh. Each cell has the algebraic versions of these transport equations applied and solved over its bounding faces so that the variance of fluid properties, such as pressure and velocity, can be calculated throughout the domain [17]. Due to the link between the discretisation process and mesh generation, the quality of a mesh plays a major role in solver stability and solution convergence, or lack thereof [18]. This means that producing a high quality mesh is critically important in realising an accurate simulation.

Historically, mesh generation was performed by mapping structured hexahedral blocks to CAD model surfaces [19]. While this is relatively easy for regular shapes that are trivial to describe mathematically [20], the process becomes highly complex when more intricate geometries are introduced. The biggest problems initially faced when meshing arise due to overly detailed CAD geometry (e.g. a car model that includes small screws and unrequired interior detail such as seats) and poorly defined CAD surfaces (those with gaps or that overlap), which are known as 'dirty CAD' [21]. These inconsistencies pose problems for automated meshing algorithms that either crash or produce poorly shaped elements to compensate. Industrial simulations tend to favour tetrahedral dominated algorithms due to their robustness and geometrical flexibility. Tetrahedra can also be combined with hexahedral elements, leading to higher resolutions and lower cell counts (for a given volume), therefore allowing for decreased computational expense and a potential time saving [22]. Also, modern software is better able to cope with dirty CAD due to functions that automatically patch small holes and remove small features that have a negligible impact on the flow [23].

2.2.2 Turbulence and its Modelling

The Reynolds number, Re, describes the ratio of inertial forces to viscous forces in a fluid.

$$Re = \frac{vl}{\nu}$$

Where l is the characteristic length, ρ is fluid density, v is fluid velocity, and ν is kinematic viscosity. For low Reynolds number flow, viscous forces dominate and flow is seen to be stable and laminar as the fluid layers move over one another in an orderly fashion [14]. When the Reynolds number exceeds a critical value, Re_{crit}, the inertia of fluid particles is great enough to overcome viscous effects. Disturbances such as obstacles and wall roughness change the direction of fluid particles and above Re_{crit} a 'turbulent' flow structure develops [15]. Turbulence is characterised by random and chaotic flow behaviour where the flow properties vary significantly and irregularly in position and time about some mean value [24]. Rotational flow structures of different sizes called 'eddies' form in turbulent flows. These eddies result in the transport of flow properties such as momentum, mass and heat. Large eddies dissipate their energy by breaking up into smaller eddies. The resulting smaller eddies break up into yet smaller eddies and this process continues until eddies have a length small enough that the viscosity of the fluid dissipates their kinetic energy as heat. The energy transfer from the largest to the smallest eddies is called the 'energy cascade' [13]. Given the

significant dynamic effects that turbulence has on a fluid flow it is important to capture these effects. The methods used to model turbulence can be grouped into three primary categories which are described briefly in the following subsections.

2.2.2.1 Direct Numerical Simulation (DNS)

Solving the discretised Navier-Stokes equations directly can capture all the minute details of a turbulent flow. For DNS to successfully model turbulence the cells of the mesh and the temporal scales must be small enough to capture the smallest scales of turbulent flow [25]. This requirement means that this method takes an enormous computational effort which makes solving practical flow problems impossible with modern day computing power. Therefore DNS applications are currently limited to small scale, simple flow problems [26].

2.2.2.2 Reynolds-averaged Navier-Stokes (RANS)

The Reynolds-averaged Navier-Stokes (RANS) are a time-averaged version of the Navier-Stokes equations which consider flow properties as a summation of the property's mean flow and its turbulent fluctuations. To form the RANS equations for a velocity vector **u**, the velocity can be decomposed into a steady state component $\bar{\boldsymbol{u}}$ and a fluctuating turbulent component $\mathbf{u}'$ that is superimposed onto it. This 'Reynolds decomposition' can be written for each velocity component as well as pressure:

Equation 1

$$\boldsymbol{u} = \bar{\boldsymbol{u}} + \boldsymbol{u}' \qquad u = \bar{u} + u' \qquad v = \bar{v} + v' \qquad w = \bar{w} + w' \qquad p = \bar{p} + p'$$

Substituting the flow variables **u**, u, v, w and p with their corresponding Reynolds decomposition before taking an ensemble average results in the so-called Reynolds-averaged Navier-Stokes equations. The averaging process results in the creation of extra stress terms in the equations which are associated with the convective momentum transfer between turbulent eddies. These extra stress terms are referred to as the 'Reynolds stresses'. In order to compute the turbulent flow behaviour using RANS equations it is necessary to model the effects of these Reynolds stresses. A number of different RANS turbulence models exist to approximate these Reynolds stresses.

2.2.2.3 Large Eddy Simulation (LES)

The behaviour of large eddies is determined by the geometry of the domain, boundary conditions and body forces. Due to these affects large eddies have anisotropic properties. RANS models consider the average behaviour of all eddies across the domain and thus the significant anisotropic effects of large eddies are not accounted for. Large Eddy Simulation (LES) uses a filter function to identify large eddies to be directly resolved and to reject smaller eddies. Applying the filter function to the continuity and Navier-Stokes equations gives LES versions of these equations. The effects of the smaller unresolved eddies are deemed to be more universal and so are included in a so-called 'sub-grid scale (SGS) model' which operates similarly to RANS turbulence models. While more accurate than RANS, the meshing requirements of LES make it a very demanding option for modelling turbulence. Near-wall cells require low aspect ratios resulting in very dense mesh regions close to wall boundaries. While a dramatic improvement in terms of computational expense compared to DNS, LES is not always practically possible for high Reynolds number flows [27].

2.2.2.4 Detached Eddy Simulation (DES)

Detached Eddy Simulation (DES), used in this project, is a Hybrid RANS-LES modelling method that uses RANS methods near walls to reduce the density of the mesh in these regions. LES is applied in other areas of the flow domain in order to better resolve the turbulent flow behaviour. Such hybrid methods must overcome issues concerning the

coupling between the two turbulence models, for example, RANS models have been shown to introduce excessive damping. An additional issue is that the time averaging used in RANS does not model turbulent fluctuations, which are difficult to reintroduce to regions modelled using LES [28].

2.3 Surrogate Modelling

CFD modelling is often very computationally expensive, especially when modelling complex flows. As a result of this computational expense, 'direct optimisation, which requires many calls to the model of interest, is more often than not, unrealistic' [29]. One technique that can be used to overcome this issue is to create a surrogate model for the CFD simulations. Surrogate models 'are constructed using data drawn from high-fidelity models, and provide fast approximations of the objectives and constraints at new design points - thereby making sensitivity and optimization studies feasible' [30]. There are several different types of surrogate model, In this project the type of surrogate model that was employed was an Artificial Neural Network (ANN). Figure 2-2 [31] is a schematic diagram of an ANN. This network consists of several layers; an input layer, one or more hidden layers and an output layer. These layers consist of interconnected neurons (or nodes) which 'can be seen as computational units that receive inputs and process them to obtain an output' [32]. The connections between the neurons are weighted and determine how the information passes through the network.

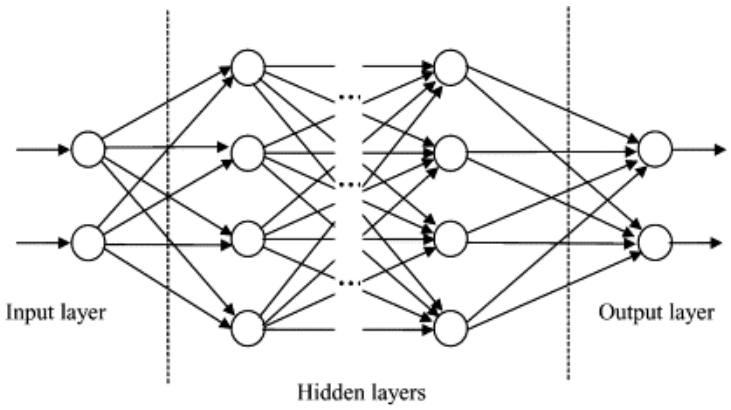

Figure 2-2 - Schematic diagram of a feed-forward artificial neural network [31]

2.4 Urban Canyon Flow

The Atmospheric Boundary Layer (ABL) is the boundary layer on the surface of the world and has an approximate thickness of 1-2km. The ABL is split into sections, one of which is the viscous sublayer (the closest 50m to the surface). Urban Canyon Flow (UCF) is the phenomenon which causes acceleration and turbulence of this sublayer. Large structures, rather than slowing the wind down, can funnel the wind into areas of high velocity and turbulence in intersections and on street corners [33], see Figure 2-3. Acceleration of the flow can also occur when wind travels downward. The three-dimensional flow is encouraged by varying building heights and is more apparent in less built-up cities. Investigations into (UCF) have been completed for multiple reasons. The two most notable of these are: for the dispersion prediction of pollutants in urban environments [34], and the optimisation of wind turbine placement in areas of high velocity [35,36].

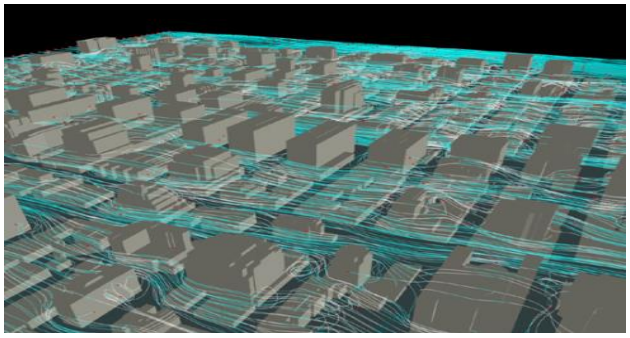

Figure 2-3 Urban wind flow in Manhattan [37]

It is expected that near street level, the velocity will be higher due to the channelling effect of the structures, however the surface roughness created by the irregularity of the area such as other cars and trees, will mean that the velocity boundary layer of the street should be large (approximately 1m). Vortices are also expected in intersections as well as on building corners.

2.5 Additive Layer Manufacture

Additive Layer Manufacture (ALM) processes involve building a component or model up layer by layer. The construction of a physical model from a CAD model by ALM processes can be broken down into a series of steps [38]. Initially the CAD file must be converted to a Stereo Lithography (STL) file, where surfaces are triangulated and the individual faces are defined through normal vectors and a list of vertices [39, 40]. The STL file is then sliced into layers before printing. Proposed methods involving the direct slicing of CAD formats have also been investigated [41, 42].

An example of an ALM process is Fused Deposition Modelling (FDM), involving the extrusion of a polymer filament through a heated nozzle. The polymer is melted and deposited onto the part, thermally bonding the layers. Support structures are required, and the technique is limited to thermoplastics such as ABS and nylon [43, 44]. The diagram in Figure 2-4 [45] describes FDM.

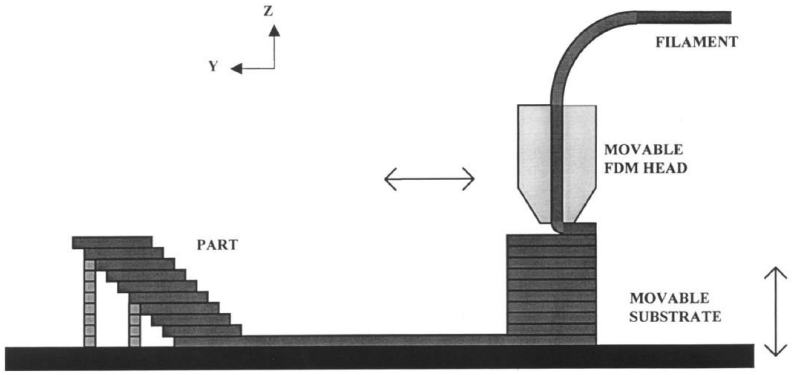

Figure 2-4 - Diagram describing the FDM process [45]

2.6 Automotive Scale Models

A common concept car design method involves the creation of three-dimensional clay models, often at scales of 1:4 or 1:2, for both aesthetic design and wind tunnel testing purposes [46]. ALM, described in the preceding section, is a rapid process which has the potential to replace traditional clay modelling techniques, leading to increased design flexibility and shortened project lead times. So far little work has been done applying ALM to produce automotive vehicle models. One example of automotive design related ALM is the

creation of a model created from gypsum and epoxy resin (of dimensions 120x45x40cm) for wind tunnel testing [47]. A photograph of this model is displayed in Figure 2-5.

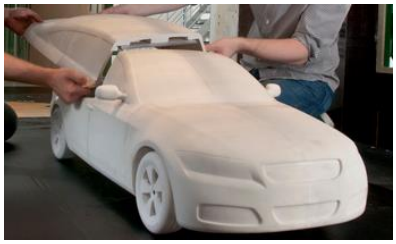

Figure 2-5 - Photograph of an ALM produced car scale model [47]

2.7 Virtual Rendering

In terms of computer graphics, rendering refers to a process by which a three-dimensional model is converted into a two-dimensional image, generally by integrating the data with respect to light physics [48]. The model incorporates geometry, lighting, texture and viewpoints to define the final image [48]. A series of these images can be combined to form animation. The remit for this part project was to render a series of still images, and create a short movie of the car driving through Exeter High Street with data collected by Walton [8]. For this project, the open-source software Blender (v2.69) was chosen, which is free for use under the GNU General Public License. Figure 2-6 shows the process flow chart.

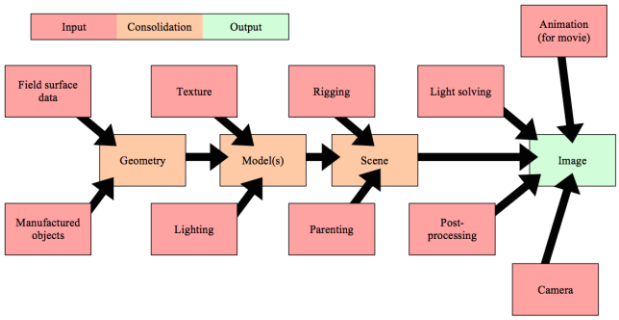

Figure 2-6 - The flow process for rendering the concept car in an environment [4]

3 Methodology

3.1 Group Methodology

Figure 3-1 is a flow chart, which highlights the major interactions between the various sub-groups during the course of this project.

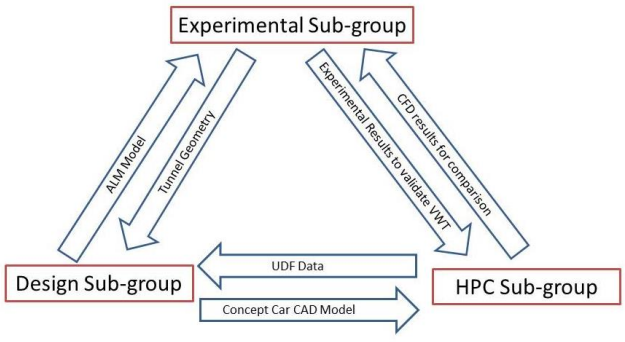

Figure 3-1 - Flow of communication between sub-groups

3.2 Concept Car Design

The aim of this project was to design a car geometry which incorporated key vehicle features to investigate aspects of computational analysis, scale model construction and wind tunnel testing. To begin with the Ahmed body was modified to include a bonnet, providing a more realistic vehicle geometry. A CAD model of the modified Ahmed body is presented in Figure 3-2.

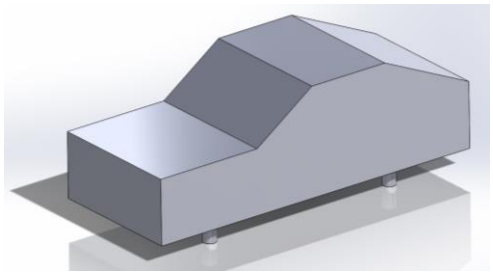

Figure 3-2 - CAD model of the modified Ahmed body [3]

Parametric CFD analysis was then conducted varying the rear slant angle [3], the front slant angle [4] and the radii of fillets added to the edges [7]. From the results of the parametric study an initial concept car was produced combining a new body profile with the modified Ahmed body, omitting complexities such as wheels. The final concept car design was created by adding realistic vehicle features including wheels, wing mirrors and a rear diffuser. CAD models of the concept cars are provided in section 4.1.

During the design process, RANS CFD analysis of the concept cars was conducted by Browne [3] to determine the drag coefficients. The RANS method was chosen because relatively accurate results could be obtained at low computational cost. The realizable k-ε turbulence model was selected because it provided improved performance for flows involving boundary layers with separation and adverse pressure gradients [49].

3.3 Scale Model Production using ALM

Three ALM processes and materials were available to produce the concept car scale models: laser sintering (nylon 12), material extrusion (ABS) and material jetting (acrylic). In order to select the most appropriate process for use in the Virtual Wind Tunnel project a matrix analysis was conducted by Browne [3], where each method was assessed against a set of criteria including cost and surface finish. From the matrix analysis it was concluded that the material jetting process was best suited to produce the concept car because it combined good geometrical accuracy, a high quality surface finish and cost effectiveness.

3.4 Rendering

The first step in the render process was to create the geometry. The concept car was built in Solidworks, while the environment was built upon surface data collected in a site visit to Exeter High Street by Walton [8]. The light source was specified as an absolute point infinitely far away, and a level of interference was added to the air to diffract the light and avoid absolute shadows [48]. Non-plain objects required UV unwrapping; this is the term for projecting a three-dimensional surface onto a two-dimensional plane [48] to apply an image or pattern onto a building, for instance. Objects can be rigged to define relationships between specified criteria of different objects; that is, it allows an applied alteration to imply another alteration on the second object. This is often used to mimic physical interactions; in this case, the wheels and tyres were rigged to the body such that movement in the local x-axis translated into rotation around the y-axis [48]. Movements were defined by inserting keyframes at

specific times. Three variables were defined in each keyframe: location, scale and rotation. Because the car was rigged, only the body needed a keyframe [48].

The final stage is the light solving, where the modelled scene results in a two-dimensional image. There are numerous methods, but the technique used for the images here is known as Cycles rendering. This works on a pixel-by-pixel basis, tracing the light path backwards from the camera to any surface, and following the diffracted light particles to their original source [48]. Because path tracing is unbiased and physically based, the result is a faithful-to-reality image. However, scenes rendered in Cycles used around 17x more CPU than the surface-based Blender Render (BI). For this reason, BI was chosen for trials and animation.

3.5 High Performance Computing (HPC)

A 3D virtual wind tunnel was developed using OpenFOAM (Open source Field Operation And Manipulations), an open source CFD code [50] together with the Ahmed body. The Ahmed body is a simplified representation of the external geometry of a car which is often used as a benchmark case for investigating automobile flow. It has a rounded front and a rear-slanted surface, the angle φ of which can be varied (see Figure 3-3 [51]). The Ahmed body was chosen to develop the VWT due to the amount of experimental and computational literature available, which could be used to validate the virtual wind tunnel generated in this project.

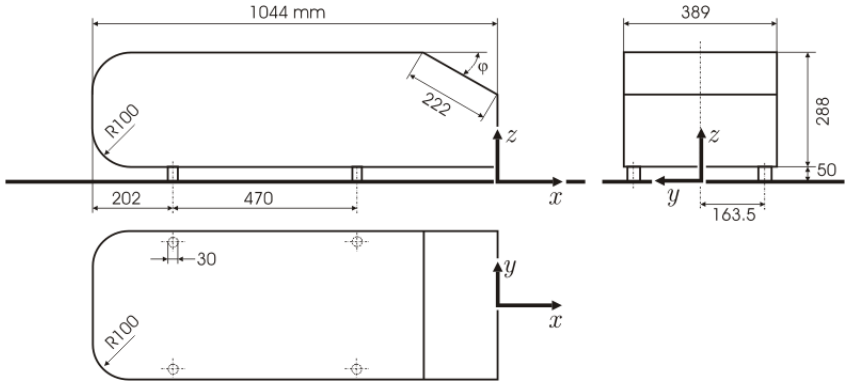

Figure 3-3 – Ahmed body model [51]

The work for the HPC group was split into three individual projects. The first individual project involved investigating the velocity flow profiles for an urban environment. The second individual project focused primarily on creating a surrogate model of the Ahmed body. This involved creating a computationally inexpensive but reasonably accurate CFD model of the Ahmed body, in order to run multiple simulations to create the data required to train an ANN. This will be referred to in this project as the 'basic CFD model'. In addition, this individual project also involved automating the CFD model and creating an ANN. The third individual project focused on creating a CFD model of the Ahmed body using more accurate and more computationally expensive methods. The main focus of this project was to use the more complex CFD Ahmed body model to develop the final virtual wind tunnel, which would then be used to test the concept car produced by the design team.

To create the CFD models of the Ahmed bodies two different meshing generation tools were investigated. The first was using snappyHexMesh - the mesh generation utility that is supplied with OpenFOAM. The second tool that was investigated was the commercial CFD meshing software, Pointwise. Several turbulence models were also investigated including the RANS turbulence models: k-ε, k-ε RNG, k-ω SST and Spalart-Allmaras. In addition a comparison was made between a DDES and an LES turbulence model. Results from different CFD simulations were compared with experimental results from the Ahmed body to determine the appropriate parameters for the final VWT such as: mesh density, turbulence model and

boundary conditions. Finally, the VWT was used to test the concept car developed by the design group.

To create the data to train the surrogate model the whole process from geometry creation to solution output was automated. The geometry creation was automated in SolidWorks [52] using DriveWorksSolo [53] (design automation software). Two parameters were varied on the Ahmed body: a fillet radius of all the sharp edges (varied from 0mm – 50mm) and the rear slant angle (varied from 5° - 45°). Thirty-five different Ahmed body models were created, and bash scripting was used to automatically mesh, solve and post process the results of these models in OpenFOAM. The bash script files created for the automated process and a description of these files can be found in Bolt [2].

In order to create a successful surrogate model of the Ahmed body, it was essential that the basic CFD model was accurate but also that it took a reasonable amount of time to run. If the model was inaccurate then there may have been little or no correlation between the input parameters and the output parameters. On the other hand, if the model was too complex then it would not have been possible to run a sufficient number of simulations to train the surrogate model. It became apparent when creating the basic CFD model that the flow around the Ahmed body was significantly more complex than expected. Consequently, far more effort was spent on producing the basic CFD model than originally intended. Due to these unexpected project delays the expertise of Richard Everson (Professor of Machine Learning at the University of Exeter) was called upon to create a surrogate model for the Ahmed body, in order to assess the feasibility of using a surrogate model in automotive design. The surrogate model was an artificial neural network that was created using the Netlab toolkit [54] in Matlab [55].

3.5.1 Modelling Urban Canyon Flow

To obtain an accurate model of the environment that the concept car will be operating in, the geometry of an urban environment needed to be taken. A crossroads in Exeter High Street was chosen for two reasons: firstly for its proximity and ease of access and secondly the intersection experiences high levels of turbulence in windy conditions creating a much more interesting model to analyse.

An Electronic Distance Machine (EDM) total station was taken to the crossroads and approximately 200 co-ordinates were collected at street level. The building heights were also calculated using the same equipment and basic trigonometry. The street and building data were interpreted by AutoCAD Civil 3D [56] and SolidWorks to create the necessary STL file for OpenFOAM. The environment, with the buildings included, was assessed using the CFD package OpenFOAM using simpleFoam and a k-ε turbulence model. The k-ε turbulence model had been successfully used by the design group in Fluent. Given successful usage of the k-ε model and RANS by the MET office in modelling the ABL for weather prediction, it was implemented for this section of the investigation [57]. The end result of the analysis was to find an inlet flow velocity user defined function (UDF) to be used in Fluent and compare the flow profiles of the concept car in uniform flow and UCF.

3.6 Experimental

3.6.1 Design Methodology

3.6.1.1 Test section Design

The final experiment was designed to make use of a formula adapted from the following equation [58]:

Equation 2

$$\frac{F_D}{L} = \rho \int_0^y U_x(U_\infty - U_x)dy$$

Where U_x is the wake velocity, U_∞ is the freestream velocity, F_D is the drag force, and y is the distance from the start of the control volume. This equation is the Von Karman Integral Formulation and allows the calculation of drag from a wake survey. This method worked with even non prismatic bodies, such as the concept car produced by the design team. This is done through an adaptation of the trapezium rule (explained fully in the results section of this report) in which rather than areas, volumes are calculated, similar to numerical double integration. In the initial tests only a single line of data points was required which was achievable with a pitot tube moving in the x-axis (horizontally, perpendicular to the flow). However, in surveying the wake of non-prismatic bodies, the wake clearly cannot be assumed to be prismatic. Therefore in the refined final experiment, a two-dimensional data set was required as the wake also varies in the y-axis (vertical). In order to calculate the drag force from this data, the wake needed to be split into small, equal areas for which the drag was calculated separately and then summed to give a total drag force. Consequently, it was decided that in a plane perpendicular to the flow, a square grid of data points would be taken that contained the whole wake of the concept car. The drag could then be calculated for each of the small square areas. The resultant system is shown in Figure 3-4, it is capable of moving along three axes in the wind tunnel in 5mm increments to tolerances of 0.01mm. A program was written in Python to control the stepper motors and position the pitot tube.

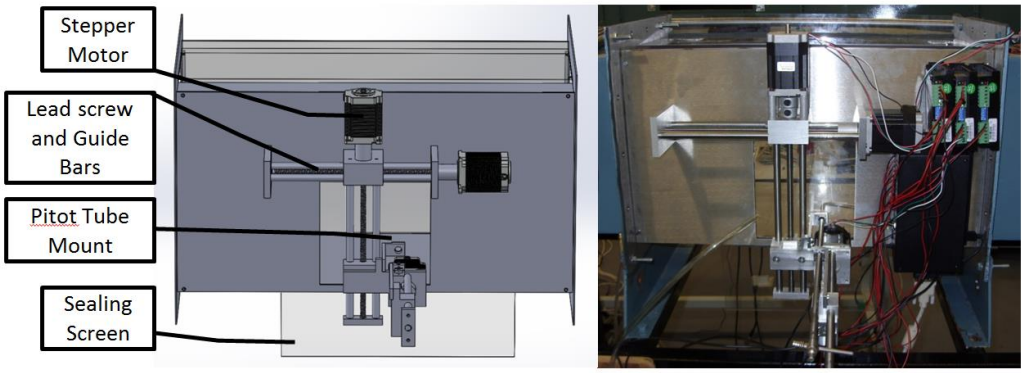

Figure 3-4- Images of final test section. Photograph of section in situ (right) and the CAD model used during its design (left)

3.6.1.2 Drag Balance Design

Another method of measuring the drag force on the model concept car experimentally is to use drag balance which was purpose built for the test section. Figure 3-5 shows the drag balance design, it consists of a nylon cable attached at one end to the model concept car and the other end to a load cell via a pulley. The drag force generated on the car by the air flow is balanced by the tension in the nylon cable, this tension is measured using an s-beam load cell bolted to the downstream flange of the test section.

One of the main advantages of this design is its versatility. The nylon cable can be detached from the load cell and attached to any type of force meter (spring newton meter, beam type load cell etc.). By using a variety of force meters multiple drag force measurements can be taken and averaged increasing the accuracy of the results. One important aspect to take note of in this design is the angle of the cable, this angle must be taken into account trigonometrically in order to determine the drag force from the tension in the cable.

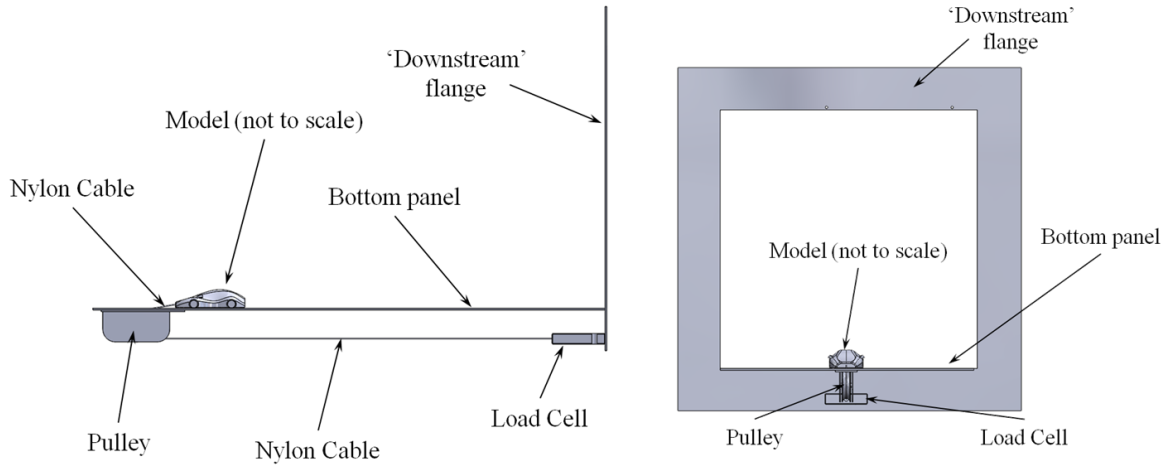

Figure 3-5: Side (left) and front (right) views of the drag balance design

3.6.2 Experimental Methods

3.6.2.1 Wake survey

The wake survey was automatically controlled through the use of a small 'Raspberry Pi' computer [59], linked to the stepper motors on the test section of the refurbished wind tunnel. The only human input required was the synchronised start of the both the python script running on the computer and the data recording software running on a separate laptop which was connected to a data logger. Once started, the program was left to run its course and the flow velocity data was exported as an HTML file. This data was then fed into a spread sheet designed process the raw velocity data into a drag force on the car as described in the results section.

3.6.2.2 Drag Balance

The experimental method for determining the drag force on the concept car using the drag balance is very simple. The cable was attached at one end to the car model and at the other end to the s-beam load cell. The output from this load cell was displayed on a data logger. The wind tunnel was switched on and brought up to speed, once at $45ms^{-1}$ the value of cable tension was noted. This test was repeated using a digital force meter, measuring load in kg to a precision of 0.01kg. The digital force meter was mounted directly below the pulley. Again, the wind tunnel was switched on and a reading was taken once it had reached $45ms^{-1}$. These drag force readings are presented and analysed in the results section.

4 Results and Analysis

4.1 Concept Car Design and ALM

A requirement from the experimental group was that the final scale model should move with minimal friction so it could be effectively tested using a drag balance. It was therefore mounted on bearings, fulfilling the specification and providing a more realistic looking vehicle model. To assess the surface finish of the material jetting process the boundary layer thickness was calculated by simplifying the case to flow over a plate. It was determined that the finish of the models was hydraulically smooth, because the estimated roughness of the surface (maximum 1mm) was less than the thickness of the theoretical boundary layer (a minimum of 1.25mm). The CAD model and the ALM printed model of the final concept car are shown in Figure 4-1.

Figure 4-1 –Final concept car, CAD model (left) and ALM printed model (right) [3]

4.2 Rendering

Following the method described in section 3.4, the concept car data was combined with field data and mesh data created in Blender. Materials and textures were created, the lighting was defined, and a virtual 20mm lens camera was deployed. The results were outputted as 4000x3000 pixel PNG images. Figure 4-2 shows such an image. The average rendering of this quality took about 90 seconds. For animation at 24fps, this translates as around 45 minutes rendering for a 5 second movie. Due to time constraints, the movies were outputted at smaller resolution. Further results and details of the process are available from Crinion [4].

Figure 4-2 - A rendered image of the concept car in Exeter High Street

4.3 CFD

4.3.1 Mesh Comparison between Pointwise and snappyHexMesh

Two different meshing tools were investigated for this project: the first was snappyHexMesh - a mesh generation tool, part of the OpenFOAM library; the second was the commercial CFD meshing software, Pointwise. A comparison was made between the meshes created in these packages by observing drag coefficients for the rear slant angles, $\varphi = 25°$ and $35°$, before comparing with experimental data .

SnappyHexMesh generated grids were used in a mesh independence study where the k-ω SST and Spalart-Allmaras (S-A) turbulence models were tested. The S-A turbulence model produced drag coefficients and flow behaviour more similar to the experimental data although these results were still in poor agreement with the experimental results [60]. Using the same numerical setup, a similar mesh convergence study was carried out for a set of grids generated

in Pointwise, which were largely unstructured but contained a structured boundary layer. The boundary layer was iteratively improved so that the first cell spacing was optimal for applying wall models. Differences between the grid structures for each method at the rear slant of the body can be seen below in Figure 4-3 and Figure 4-4.

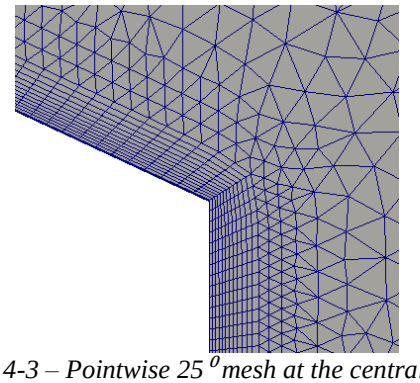

Figure 4-3 – Pointwise 25 ^{0} mesh at the central plane of the rear slant ($1.8x10^{6}$) elements)

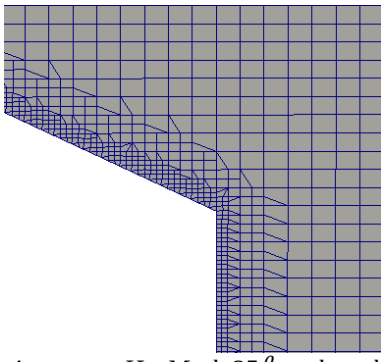

Figure 4-4 – snappyHexMesh 25 ^{0} mesh at the central plane of the rear slant ($2.5x10^{6}$ elements)

The convergent drag value for the Pointwise meshes showed better agreement with the experimental results than the grids generated by snappyHexMesh. The computed drag coefficients are presented in Table 4-1. The error results suggest that the accuracy of the drag coefficient is impaired by the limited quality of the boundary layer region. It was noted that neither mesh correctly predicted the drop in drag between 25° and 35° rear slant angles observed experimentally.

Table 4-1 – Converging C_d for snappyHexMesh and Pointwise meshes against experimental C_d using S-A

Rear Slant Angle	Experimental Drag Coefficient C_d	Meshing Program	Computed Drag Coefficient C_d	Error % (compared to experimental)
25°	0.299	snappyHexMesh	0.351	17.4%
		Pointwise	0.335	12.0%
35°	0.279	snappyHexMesh	0.395	41.6%
		Pointwise	0.354	26.9%

A comparison between velocity vector plots for the two meshes at φ =25° showed that Pointwise meshes more accurately predicted the near-wake flow structures seen in the experimental work. The Pointwise grid correctly suggested complete separation over the rear slant, where the snappyHexMesh did not. The improved flow topology and drag coefficient results of the Pointwise meshes illustrated the importance of the boundary layer mesh quality.

Owing to its improved accuracy and mesh control, the Pointwise meshing method was carried forward for the development of the VWT. While the results of the Pointwise grids more accurately replicated the experimental results, the ability to automate mesh generation in snappyHexMesh made the meshing process far less time-consuming. In order to generate a sufficient set of data for the surrogate model to learn from (in the limited time frame of the project) the snappyHexMesh method was carried forward.

4.3.2 RANS and DDES Turbulence Models

A structured mesh was generated to observe the impact this had on the accuracy and stability of the solutions. It was found that applying second-order central differencing schemes to the hybrid meshes resulted in divergence where the structured mesh converged successfully to residuals in the order of 10^{-5}. The resulting drag coefficients when using a second-order differencing scheme with an unstructured mesh were seen to accurately predict the drag

coefficients as illustrated in the error between the computational and experimental results in Table 4-2.

Table 4-2: RANS drag coefficients for structured meshes using second order differencing

Rear Slant Angle	Experimental Drag Coefficient C_d	Turbulence Model	Computed Drag Coefficient C_d	Error % (compared to experimental)
25°	0.299	k-ω SST	0.278	-7.0%
		S-A	0.292	-2.3%
35°	0.279	k-ω SST	0.279	0%
		S-A	0.294	5.4%

Despite generating promising results for drag coefficients, the k-ω SST turbulence model was observed to incorrectly suggest complete separation over the rear slant angle φ = 25°. It was concluded that the most reliable and accurate RANS turbulence model for predicting the drag coefficient and rear-wake behaviour over the Ahmed body was S-A using a structured grid.

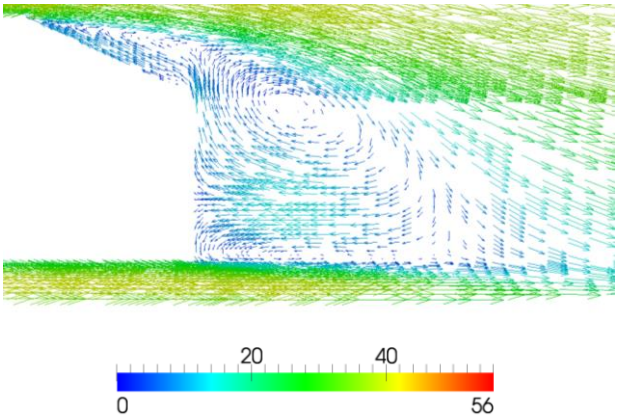

Figure 4-5: Incorrect flow separation for φ =25° (U magnitude, m/s)

The DDES results were initialised using the S-A RANS case results to reduce the computation time associated with reaching steady-state. A time step of $5x10^{-6}$s was used in order to keep the courant number of the transient simulation below approximately 0.5. The time averaged drag coefficients are presented in Table 4-3. While the error of these drag coefficients was greater than for the steady-state RANS case, the DDES turbulence model was the only one to correctly predict the reduction in drag between φ = 25° and φ = 35°. In spite of the substantial error in computed drag coefficients, the time-averaged results more accurately represented the topology of the recirculation zones in the near wake region. The drop in drag and improved time-averaged flow prediction suggests that the anisotropic effects of the eddies in the near-wake region need to be considered in order to accurately describe the different flow regimes observed experimentally.

Table 4-3: DDES drag coefficients for structured mesh using second order differencing

Rear Slant Angle	Experimental Drag Coefficient C_d	Turbulence Model	Computed Drag Coefficient C_d	Error %
25°	0.299	DDES	0.341	14.5%
35°	0.279	DDES	0.294	5.4%

4.3.3 Advanced Meshing Strategies

To assess how effectively the CFD simulation procedure could be integrated into the automotive design process, the speed and accuracy of a variety of meshing strategies were investigated in Fluent. A mesh convergence study using four different meshing schemes was run in Fluent for the flow past an Ahmed body, of rear slant angle 25°, within a VWT. There were two different types of meshes: Patch-Dependent (PD) and Patch-Independent (PI). The former technique builds meshes based upon the input geometry, whereas the latter is more robust as it infers geometry location from where the generated volume mesh meets the CAD surfaces, and so is not reliant on the CAD being of good quality. PD included fully tetrahedral and hybrid (tetrahedral with wedge element inflation layers), PI included 'Cut-Cell' (mostly hexahedral with wedges and tetrahedra also) and fully tetrahedral.

Each study used largely the same face sizing graduation and nine iterations to increase the mesh density, on average, from 23,000 to 4 million elements. Solver settings were also kept almost identical to ensure that valid comparisons could be made between the schemes. Figure 4-6 gives the graph of change in drag coefficient with increasing mesh density for each meshing scheme, compared to Meile's [60] experimental result of C_d = 0.299 for a 25° rear slant angle.

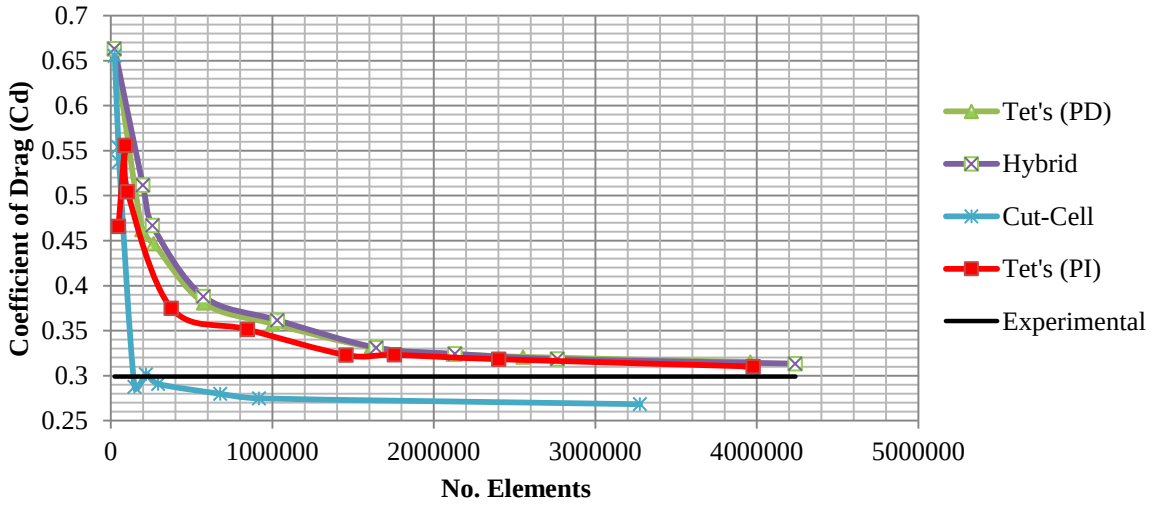

Figure 4-6 - Comparison of mesh convergence studies for four meshing schemes on drag coefficient with experimental result of Ahmed body with rear slant angle = 25°. PI =Patch-Independent, PD=Patch-Dependent.

It can be seen that PD tetrahedral and hybrid meshes converge on an almost identical solution with the same mesh density, whereas the cut-cell mesh produces a less accurate result for a similar mesh density, and overall the PI tetrahedral is the most accurate once converged. Furthermore, due to convergence issues, the solving scheme for the cut-cell method was changed from 1st to 2nd order after the first 100 iterations for each mesh in the study. The results are unusual since 1st order schemes are supposedly more stable and less accurate than 2nd order but the opposite of this was seen for the cut-cell method. This is likely due to the mesh's interaction with the solver and because cut-cell methods are relatively new to CFD, and so may still be in development. Furthermore, convergence times were recorded for each mesh within each scheme and it was clear that the cut-cell method took longer to produce a less accurate solution than the other methods, for a given mesh density. This makes it an unattractive choice for CFD meshing at present. The PI tetrahedral was again the leader here and produced the most accurate meshes in the least time for a given mesh density. Lastly, changes in average and extrema values for three quality metrics were recorded for each mesh in each study, which were: equiangle skewness, aspect ratio and orthogonal quality. However,

there was little, if any, correlation between increasing mesh density and negative repercussions in terms of average element quality. There was also little association between meshes having a supposedly low quality and comparable solution stability or convergence time.

4.3.4 Surrogate Modelling

In order to investigate the surrogate modelling process, two input parameters for the Ahmed body were varied: a fillet radius of all the sharp edges and the rear slant angle. One output parameter – the drag coefficient – was recorded. Using the automated process outlined in methodology, 35 different CFD models were run using seven different rear slant angles (5°, 12.5°, 20°, 25°, 35°, 40°, 45°) and five fillet radii (0mm, 7.5mm, 15mm, 30mm, 50mm). The CFD models were run in OpenFOAM using the S-A turbulence model, simpleFoam solver, and mesh density of 2.5million elements (generated using snappyHexMesh). The total time for these simulations was 55 hours when running in parallel on 12 cores @ 3.47GHz. A surface plot of the results can be seen in Figure 4-7. This data was then used to train a type of Artificial Neural Network (ANN) known as a multi-layered perceptron (MLP). As discussed in the methodology section the ANN was created and optimised by Richard Everson (due to project delays) - see Bolt [2] for a description of the optimisation process. The optimised ANN was able to predict the drag coefficient with an average error of 2.3%. After the ANN had been trained, 600 data points (i.e. a fillet radius and a rear slant angle) were randomly generated, this information was provided to the trained ANN and the drag coefficient was predicted for these points – the results are shown in a surface plot (see Figure 4-8). It took just under three minutes to train and optimise the ANN, and then predict the drag coefficient for these 600 points. However it would have taken around 39 days to run the same 600 points as CFD simulations under the same conditions described above (12 cores running in parallel @ 3.47 GHz). These results have shown that for two input parameters a surrogate model has been able to accurately predict the drag coefficient for the Ahmed body, at a computational expense that is significantly less than a CFD model. This indicates that automotive design optimisation studies may be possible using a surrogate model where it would have been impossible otherwise.

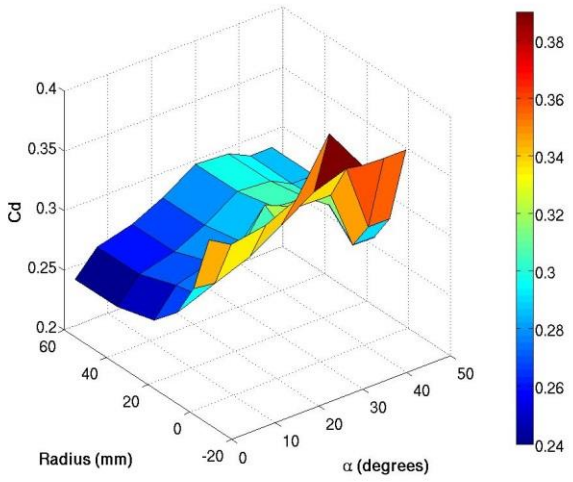

Figure 4-7 - surface plot of drag coefficient plotted against fillet radius and rear slant angle (CFD results)

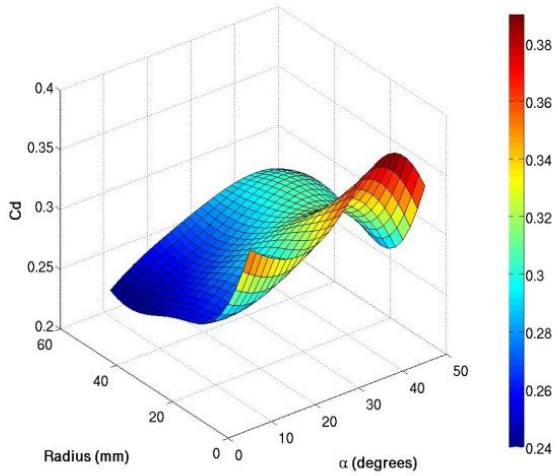

Figure 4-8 - surface plot of drag coefficient plotted against fillet radius and rear slant angle (ANN results)

4.4 Urban Canyon Flow

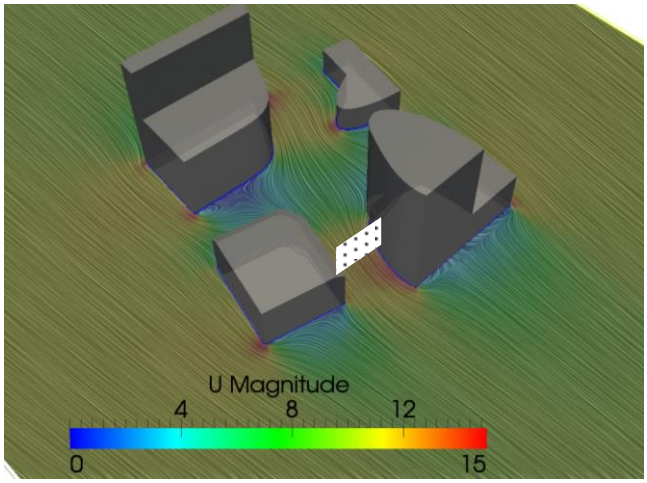

Figure 4-9 -Flow velocity vectors at a height of 1m

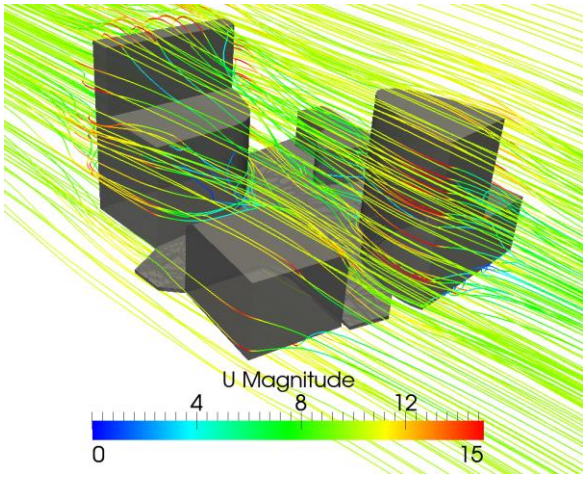

Figure 4-10 Whole domain velocity streamlines

Exeter high street exhibited classic urban canyon characteristics. There are high levels of turbulence in the intersection as well as flow acceleration in the narrow spaces of the streets and around the corners of the buildings, seen in Figure 4-9 and Figure 4-10. Vortices also form in the wakes of the buildings. An array of probes was placed in the model to record velocity for post processing, the location can be seen in Figure 4-9, symbolised by the white region. The velocity values were plotted against the z-coordinate (height), to generate a velocity profile as seen in Walton [8]. A polynomial equation was found from these points and used as a UDF for Fluent.

Equation 3

$$x = 0.506y^6 - 5.0841y^5 + 17.562y^4 - 22.423y^3 + 0.0843y^2 + 16.885y + 4.4157$$

Velocity streamline plots of uniform and the parabolic flow profiles can be seen below in Figure 4-11, obtained from Browne [3]. It can be seen that the plot with the UDF has a far more turbulent wake and vortex shedding occurring at rear of the car. The fact that the velocity plots are drastically different demonstrates that a change in environment can increase the drag on a vehicle. The drag for uniform flow was 10.9N and the drag for the UDF inlet was 14.5N.

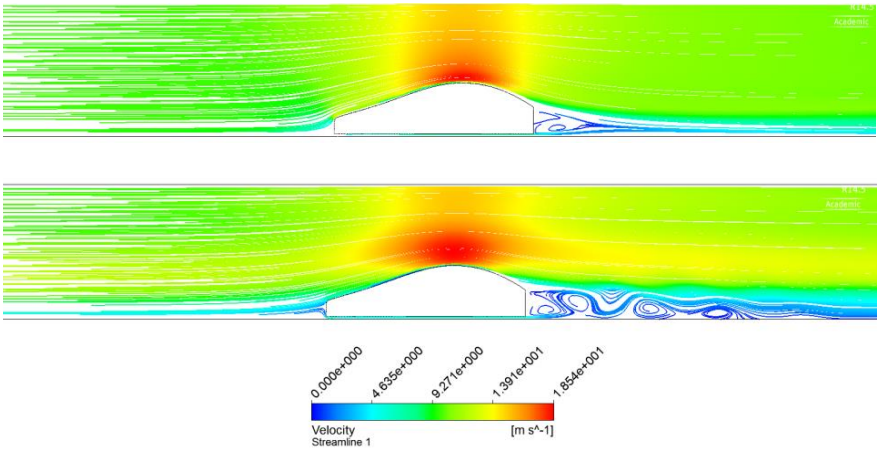

Figure 4-11 - Velocity Profile from the UDF (bottom), Velocity Profile from a Uniform 10m/s inlet (top)

4.5 Virtual Wind Tunnel Validation and Experimental Results

4.5.1 Experimental Results

4.5.1.1 Drag Balance

From the experimentation described in section 3.7.2.2, two values of drag force were obtained, more detail about the experimental errors can be found in Docherty [5]:

- S-beam load cell: 0.49N ± 0.005N
- Force meter: 0.39N ± 0.049N

The angle of the cable was determined by measuring the horizontal and vertical distances from the pulley to the mounting point on the car model. The mounting point was 290mm back from the pulley and 1.99mm high. The angle can simply be found from trigonometry to be 0.39^0; this is small enough that its effect on the results is negligible.

The coefficient of drag is related to the drag force by the equation below [61]:

Equation 4

$$C_d = \frac{F_d}{0.5 \times \rho U^2 A}$$

Where Cd is the drag coefficient, F_d is the drag force (shown above), ρ is the density of air (1.2 kgm^{-3} at 20.5°C), U is the air velocity (45ms^{-1}) and A is the frontal area (determined from the CAD model to be 2932.92mm^2). Substituting these values into Equation 4 give the drag coefficients below:

- $C_{d\ load\ cell} = 0.18 \pm 0.003$
- $C_{d\ force\ meter} = 0.15 \pm 0.027$

To improve the accuracy of the results the mean of these two values was found, therefore the coefficient of drag found using the drag balance was 0.17 ± 0.015 (2 significant figures).

4.5.1.2 Wake Profile Survey

The drag force found using the wake survey method detailed in section 3.7.2.1 was F_D = 1.19N. The car was tested at an angle 14° as the drag balance pulley and pitot tube interfered with the positioning of the car. Using equation 1, the drag coefficient was calculated as $C_{d\ Wake\ Survey} = 0.358$ This was found by discretising the Von Karman integral formulation (given in Equation 2) on a square grid of data, collected using the renovated wind tunnel test section. A wake survey was performed in which velocity data was taken for every point in a 5mm grid measuring 140mm by 50mm. Individual momentum losses were calculated for each 25mm^2 area in the wake. The graphs in Figure 4-12 show the distribution of momentum loss over the whole wake of the concept car. The total loss of momentum in the control volume was calculated by summing the losses from the small areas. By the principle of conservation of linear momentum, the amount of drag force on the car is equal to the momentum change in the flow.

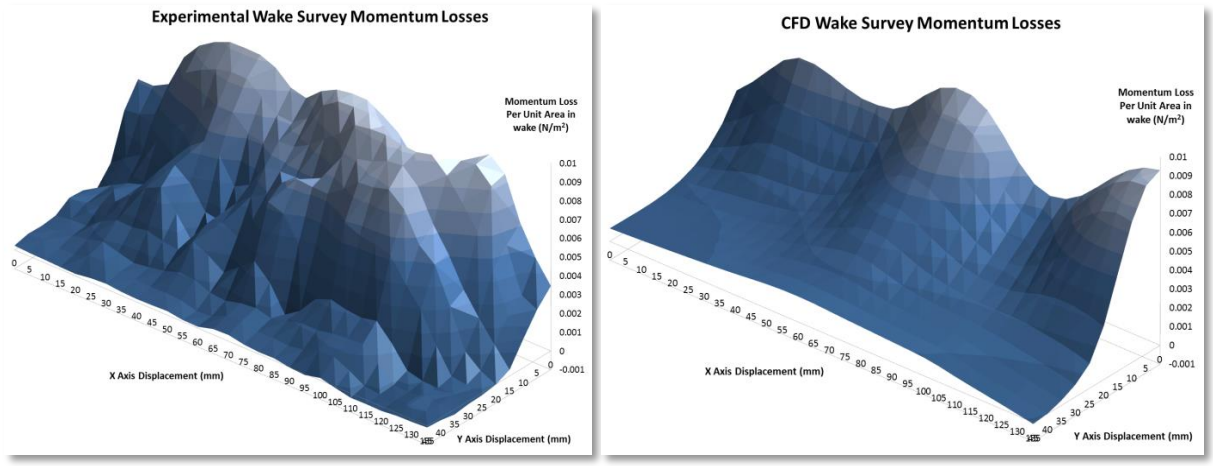

Figure 4-12- Surface plots of momentum loss per unit area in the wake survey with experimental results (left) and VWT results (right) [1]

4.5.2 Concept Car Virtual Wind Tunnel Results

The experimental arrangement of the wind tunnel and concept car were represented in a 3D CAD model so that the domain could be meshed. The setup of the RANS S-A simulations were adapted to consider the boundary conditions of the experimental setup. The wind tunnel was enclosed by no-slip wall boundaries on all sides. The velocity at the inlet was calculated to conserve mass flow rate by considering the velocity of the air in the test section, which was measured as 38.88m/s. Mesh generation was found to be extremely difficult given the complex and detailed geometry of the car. It was found that the Fluent PI tetrahedral mesh predicted a similar drag coefficient to that indicated by the drag balance; these were 0.167 and 0.17± 0.015 respectively.

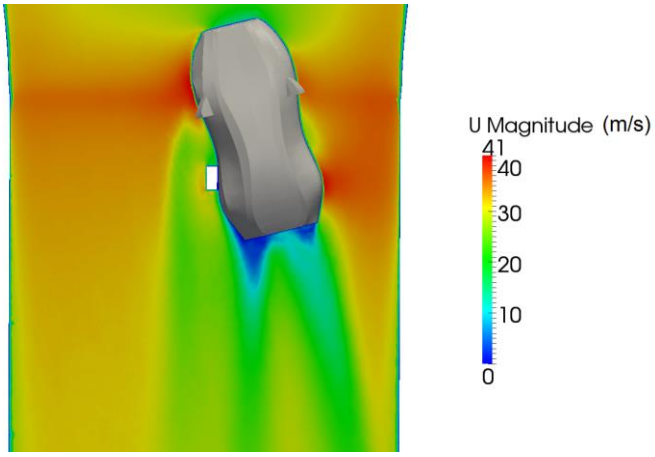

Figure 4-13 – Velocity contour plot at y = 15mm

The momentum loss plots shown in Figure 4-13 (section 4.5.1.2) showed a general agreement between the momentum loss measured experimentally and that using the VWT. The experimental method recorded 3 values of velocity at each data point over 3 seconds which were then averaged. The transient turbulent effects in the wake region caused these values to vary over a large range, and thus with only 3 data readings, it was difficult to obtain accurate average solutions. The resulting momentum loss plot therefore shows more random fluctuations between neighbouring data points than for the steady-state RANS results. The three peak values of momentum loss observed in the plots correlate to the regions of lower flow rate visible in the wake of the vehicle seen in Figure 4-13 which corresponded to trailing vortices. Drag coefficient was calculated to be 0.358 using considering momentum loss where experimental results predicted a drag of 0.298.

5 Management

5.1 Economic Analysis

A budget of £100 per head was provided by the University of Exeter. However, there were some group members that required no funding, as some of the group's work was purely computational. The £100 per head was amalgamated into an £800 group fund. A treasurer was assigned to be responsible for keeping track of group expenditure. A breakdown of the costs is shown below in Table 5-1. While £58.96 over budget the group has provided the University with a robust wind tunnel designed with longevity in mind which will benefit the department in the foreseeable future.

Table 5-1 - Total Expenditure breakdown of the group

Reason for Expenditure	**Cost**
Experimental computing equipment	£349.97
Experimental Stainless Steel	£221.92
Travel to Southampton University- expert consultation	£40.00
ALM concept cars	
First Concept Car	£117.03
Second Concept Car	£130.04
Total	£858.96

5.2 Time Management

The project length spanned 7 months (October to April) and a Gantt chart was used to plan and monitor the time management and progression of the whole group (see group logbook). The group had several forms of communication and organisation. The main form of communication between group members were weekly one hour meetings, with the project supervisor, to see the progress of each member as well as assess any problems or hindrances in the whole project. Minutes were taken (see logbook for examples and details) by the secretary for every meeting and the proceedings were led by the Chair, both of these roles rotated on a weekly basis. Towards the end of the investigation, a project co-ordinator was assigned to oversee the progress, and organise meetings and report collaboration. The group logbook was kept not only for the meetings but also for writing down suggestions from visiting professionals and comments from the project supervisor.

Electronic communication was also used by the group for the exchange of information between weekly meetings. Shared cloud-based storage was implemented to contain all of the group's files and also to share necessary research papers that will be relevant to all members. As well as this a Social Media group was created for discussion and organisation between meetings.

5.3 Health and Safety

A risk assessment was completed for all aspects of this project including: practical, field and desk work. The completed risk assessment can be found in the group log book.

6 Sustainability Analysis

This section is a discussion of the environmental implications of the project, including energy consumption and recyclability of the materials used in concept car production. It also includes a hypothetical sustainability analysis of industrial use of ALM to create wind tunnel models.

6.1 ALM in Industry

Due to the minimal loading on wind tunnel models, the fastest and most sustainable ALM processes could be chosen to form them. Such processes include Stereolithography, Selective Laser Sintering and 3D Printing which use photo-curing resin, thermoplastics and a plaster/resin composite respectively. ALM processes like Selective Laser Melting allow for the use of stronger materials at the cost of a slower build time and larger energy consumption required to melt these materials.

The models produced during this project were small in comparison to the ¼ size models commonly used in the automotive industry, consequently the environmental impact of the choice of ALM process for these models was deemed negligible. If ALM were used to create larger models, the thickness of the shells would also need to increase to support the increased weight of the part. Therefor factors such as material melting point and build time could have large impacts on the energy requirements of the car design process.

Material recyclability and wastage of the chosen ALM process should also be considered if it were to be implemented on an industrial scale. Due to the high temperature gradients in the parts throughout manufacture, certain processes require the use of "support structures" to conduct the excess heat away to prevent warping. These support structures and any old car models can be melted down for reuse with some processes. In industry this is more an environmental concern than an economical one.

Figure 6-1 is a graph of the specific energy consumption and build rate of various industrial ALM processes [62]. As seen in Figure 6-1 the lowest energy processes are: A1 (Electron Beam Melting), SLM250 (Selective Laser Melting), EOSINT P 390 (Selective Laser Sintering). Of these, A1 is the fastest with the lowest energy but produces a rough surface finish which may affect wind tunnel data. Therefor a secondary operation would be required to ensure that the flow around them was realistic. The energy consumption of this secondary operation would also need to be considered. If an effective finishing process could be developed to smooth the surface, this process would be ideal for use in industry.

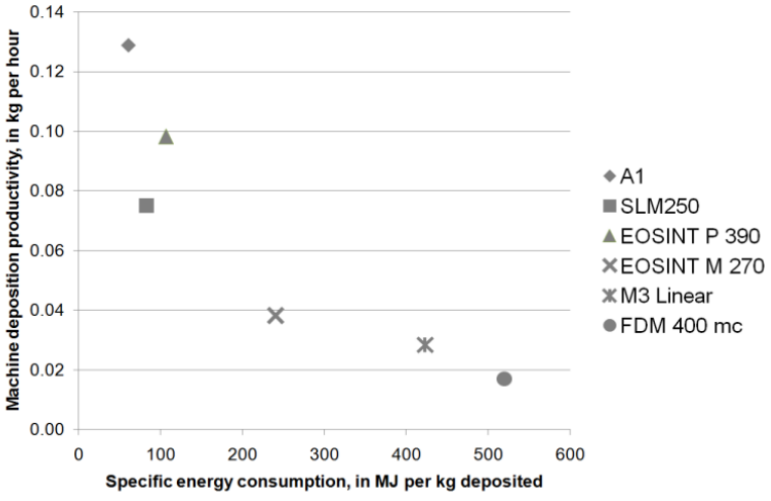

Figure 6-1 - Graph to show the energy consumptions and printing speeds of various ALM techniques

6.2 Project Energy Consumption

The following is a comparison of the amount of energy consumed by both the experimental and HPC methods employed during this project. The wind tunnel operates at 480 Volts with a

current of 8.4 Amps at maximum speed. This gives a power of 4.116kW. The wake survey performed by the experimental group took 1 hour 40 minutes. This gives a total energy consumption of 6.85kWh. The concept car tested in the wind tunnel was produced using a process similar to FDM, which from Figure 6-1, uses 520 MJ per Kg of material deposited. The car weighed 50g and therefor took 7.2 kWh of energy to produce.

The computers on which the CFD calculations were performed are supplied by a 900W power supply unit. However, this is the maximum power available and it typically not required. Power consumption readings of 260W were taken for the processor during a simulation. To obtain the required result, this 1.5 day simulation was repeated 4 times, for a total power consumption of 4.68kWh. Comparing the energy consumption of VWT use and wind tunnel wake surveys, clearly the VWT is more sustainable as it requires only 4.68kWh to obtain the data required. The ALM model and wake survey combined required 14.05kWh to create a 319 data point wake survey, although the model could be reused for further testing.

7 Conclusion

In conclusion, this group project has investigated the integrated design approach to create the external body of a concept car using CAD, CFD and wind tunnel testing. The Design Group has iteratively designed a concept car using CFD and CAD. This concept car was manufactured using ALM to be tested in the wind tunnel. It was found that ALM has the potential to reduce project lead times and increase design flexibility, making it a viable alternative to clay scale models. The concept car was also virtually rendered using Blender in a realistic environment built using data gathered from an Electronic Distancing Machine.

The Experimental group has redesigned and manufactured a test section for an open-circuit wind tunnel. It was used to find the drag coefficient of the concept car using a drag balance and velocity wake survey. The test section manufactured was able to automatically generate a grid of data points to an extremely high precision. An automated probe positioning mechanism was created by using a Raspberry Pi computer module to control a stepper motor array. The force on the car was measured using a drag balance which gave drag coefficients of 0.17 ± 0.015. A velocity wake survey was also conducted for the car at an angle of 14° off the stream-wise axis; this was used to calculate a drag coefficient of 0.358 using Von Karman's integral formulation.

HPC has been implemented to validate a numerical setup and meshing techniques for use within a VWT that utilised CFD. Experimental data for an Ahmed body has been used to validate the final case setup. The case used the Spalart-Allmaras RANS turbulence modelling and second-order central differencing with a structured mesh. This setup calculated drag coefficients to within 5.4% of the experimental data. Applying the VWT to the concept car case gave drag coefficient results for the off-axis scenario of 0.298 (compared to 0.358 found experimentally). Patch independent tetrahedral meshing in Ansys Fluent was able to generate a mesh of acceptable quality which was used to generate a result similar to the experimental drag coefficient; with the simulation predicting 0.167 against the experimental result of 0.17 ± 0.015. A surrogate model was created for the Ahmed body which was able to accurately predict the drag coefficient for a varying fillet radius and rear slant angle with an average error of 2.3%. This model generated results at a computational expense that was significantly lower than the CFD model on which it was based. Urban flow profiles were also investigated to observe their effects on the drag. It was found that the urban flow profile had a significant effect on the near-wake region and this resulted in a higher drag force on the car than observed in a uniform flow.

8 References

[1] Blades, L., 2014. *Individual Report I2: Virtual Wind Tunnel Project.* MEng Report. University of Exeter

[2] Bolt, H., 2014. *Individual Report I2: Virtual Wind Tunnel Project.* MEng Report. University of Exeter

[3] Browne, F., 2014. *Individual Report I2: Virtual Wind Tunnel Project.* MEng Report. University of Exeter

[4] Crinion, E., 2014. *Individual Report I2: Virtual Wind Tunnel Project.* MEng Report. University of Exeter

[5] Docherty, D., 2014. *Individual Report I2: Virtual Wind Tunnel Project.* MEng Report. University of Exeter

[6] Hamilton, L., 2014. *Individual Report I2: Virtual Wind Tunnel Project.* MEng Report. University of Exeter

[7] Nima, D., 2014. *Individual Report I2: Virtual Wind Tunnel Project.* MEng Report. University of Exeter

[8] Walton, J., 2014. *Individual Report I2: Virtual Wind Tunnel Project.* MEng Report. University of Exeter

[9] ANSYS, Inc., ANSYS FLUENT (Version 14.5) [Computer program]

[10] Pointwise Inc. Pointwise (V17.1 R4) [Commercial Meshing Software]

[11] OpenFOAM Foundation, OpenFOAM (Version 2.2.2) [Open Source CFD code] Available at: http://www.openfoam.com/

[12] Pankhurst, R. C, Holder, D.W. (1952) *Wind-Tunnel Technique*. London: Sir Isaac Pitman & Sons Ltd

[13] Versteeg, H. K. and Malalasekera, W., 2007. *An introduction to computational fluid dynamics: the finite volume method*, 2nd ed. Harlow: Pearson Prentice Hall.

[14] Anderson, J.D., 2009. *Computational Fluid Dynamics*. 3rd ed. Berlin: Springer. pp.15-51.

[15] Sayma, A., 2009. *Computational Fluid Dynamics*. Ventus Publishing. pp. 8-9.

[16] Ashgriz, N. and Mostaghimi, J., (no date). *An Introduction to Computational Fluid Dynamics*. Toronto: University of Toronto. pp.2-21.

[17] Cengel,Y.A., Cimbala, J.M. (2006). *Fluid Mechanics: Fundamentals and Applications*. New York: McGraw-Hill. pp. 818-216.

[18] Juretic, F. (2004). *Error Analysis in Finite Volume CFD*. Ph.D Thesis. London: Imperial College London. pp. 43-66

[19] Thompson, J.F., Soni, B.K., Weatherill, N.P. (1999). *Handbook of Grid Generation.* New York: CRC Press LLC. pp. 29-44.

[20] Kovacevic, A, Stosic, N, Smith, I. (2007). *Screw Compressors: Three Dimensional Computational Fluid Dynamics and Solid Fluid Interaction.* London : Springer-Verlag. pp. 42-45.

[21] DEStech Publications, Inc**.** (2010). *Parallel Computational Fluid Dynamics: Recent Advances and Future Directions.* Lancaster : DEStech Publications, Inc. pp. 44-47.

[22] Bakker, A.(2006). *Computational Fluid Dynamics: Course Materials and Lectures.* [Online]. [Cited: 15 03, 2014.] http://www.bakker.org/dartmouth06/engs150/.

[23] Ansys. *Fast, Robust, Automatic Mesh Creation for CFD.* [Online] 2014. [Cited: 08 04, 2014.]http://www.ansys.com/Products/ANSYS+15.0+Release+Highlights/Fluids/Fast,+Robust,+Automatic+Mesh+Creation+for+CFD+15-0

[24] Pope, S.B., 2000. *Turublent Flows*. Cambridge University Press: Cambridge.

[25] Utah University. (no date). *Length and Time Scales in Turbulent Flows.* Available at*:* <http://www.eng.utah.edu/~mcmurtry/Turbulence/turblt.pdf>. Accessed on 07 December 2013

[26] Moro-Ludena, D., 2013. *A Reynolds-Averaged Navier-Stokes solver with transition prediction capabilities*. MIT.

[27] Tessicini, F., Leschziner, M.A., 2008. Wall-modelling strategies in large eddy simulation of separated high-Reynolds-number flows. Sponsored Research Paper for BAE Systems. Imperial College.

[28] Gaitonde U., 2008. *Quality Criteria For Large Eddy Simulation.* First year PhD Report. Submitted to the University of Manchester.

[29] Leary, S. J., Bhaskar, A., Keanea, A. J., 2004. A Derivative Based Surrogate Model for Approximating and Optimizing the Output of an Expensive Computer Simulation. *Journal of Global Optimization*. **30**, pp. 39–58.

[30] Queipo, N. V., Haftka, R. T., Shyy, W., Gol, T., Vaidyanathan, R., Tucker, P. K., 2005. Surrogate- based analysis and optimization. *Progress in Aerospace Sciences.* **41,** pp. 1-28.[

[31] Kalogirou, S. A., 2001. *Artificial neural networks in renewable energy systems applications: a review.* Renewable and Sustainable Energy Reviews **5**(4): 373-401.

[32] Gershenson, C., 2013, *Artificial Neural Networks for Beginners.* [online] Available at: http://arxiv.org/ftp/cs/papers/0308/0308031.pdf [Accessed 11/11/2013].

[33] Zajic D., Fernando H.J.S. and Brown M.J, 2010. Flow and Turbulence in an Urban Canyon, Department of Mechanical Engineering, University of California

[34] Chang, C.-H. and Meroney, R., 2003. Concentration and flow distributions in urban street canyons: wind tunnel and computational data
[35] Rotach, M and Zardi, D., 2007. On the boundary-layer structure over highly complex terrain: Key findings from Map Quarterly Journal of the Royal Meteorological Society
[36] Holdaway, D., Tabor, G. and Beare, B., (2013) An Examination of the Feasibility of Using OpenFOAM to Model Air Flow for Wind Turbine Positioning, The University of Exeter
[37] wordpress.com, 2011. Air Flow in Manhattan, How it affects the urban population and how it can be used beneficially. [Accessed 19/04/14]. Available at: http://fungsiangtai.wordpress.com/2011/11/09/assignment4-revised-air-flow-in-manhattan-how-it-affects-the-urban-population-and-how-it-can-be-used-beneficially/
[38] Gibson, I., Rosen, D.W., Stucker, B. 2010. *Additive Manufacturing Technologies Rapid Prototyping to Direct Digital Manufacturing.* Springer.
[39] Fadel, G.M., Kirschman, C., 1996. Accuracy issues in CAD to RP translations. *Rapid Prototyping Journal*, 2(2), pp4-17
[40] Bianconi, F., 2002. Bridging the gap between CAD and CAE using STL files. *International Journal of CAD/CAM*, 2(1), pp55-67
[41] Wang, W.C., Gu, H.X., 2011. Direct Slicing of CAD Model and Volumetric Error Compensation in Rapid Prototyping. *Advanced Materials Research*, 317-319, pp1598-1602
[42] Jamieson, R., Hacker, H., 1995. Direct slicing of CAD models for rapid prototyping. *Rapid Prototyping Journal*, 1(2), pp4-12
[43] Kalpakjian, S., Schmid. S.R., 2001. *Manufacturing Engineering and Technology*. 4th Edition, Prentice Hall.
[44] Yan, Y., Li, S., Zhang, R., Lin, F., Wu, R., Lu, Q., Xiong, Z., Wang, X., 2009. Rapid Prototyping and Manufacturing Technology: Principle, Representative Technics, Applications, and Development Trends. *Tsinghua Science and Technology*, 14(S1), pp1-12
[45] Pham, D.T., Gault, R.S., 1998. A comparison of rapid prototyping technologies. *International Journal of Machine Tools & Manufacture*, 38(10-11), pp1257-1287
[46] A. Gaylard, 2014. *Discussion on automotive design processes*. [Personal communication 06/03/2014]
[47] 3ders.org, 2012. *3D printed car model DrivAer as a key to vehicle air circulation*. [online] Available at: <http://www.3ders.org/articles/20120907-3d-printed-car-model-drivaer-as-a-key-to-vehicle-air-circulation.html> [Accessed 04 April 2014]
[48] Hess, R. 2010. *Blender Foundations: The Essential Guide to Learning Blender 2.6*. Focal Press.
[49] Fluent Inc., 2006. *Fluent 6.3 User's Guide* [online] Available at: <http://aerojet.engr.ucdavis.edu/fluenthelp/html/ug/main_pre.htm> [Accessed 11 April 2014]
[50] OpenFOAM Foundation, OpenFOAM (Version 2.2.2) [Open Source CFD Code] Available at: http://www.openfoam.com/ [Accessed 17/04/2014]
[51] CFD Online, 2005. *File:Ahmed.gif.* [online] Available at: http://www.cfd-online.com/Wiki/File:Ahmed.gif [Accessed 28/09/2013].
[52] Dassault Systèmes, Solidworks (Version 2014) [Computer program]
[53] DriveWorks Ltd, DriveWorks Solo [Design Automation Software for use in SolidWorks]
[54] Nabney, I., Bishop, C., Netlab [Matlab functions and scripts]
[55] Mathworks, Matlab (R2012a) [Computer program]
[56] AutoCAD Civil 3D, Autodesk (2015) [Computer Prgram]
[57] Calvert, D., Siddorn, J., 2013, Revised vertical mixing parameters for the UK community standard configuration of the global NEMO model Available at : http://www.metoffice.gov.uk/media/pdf/9/0/HCTN_95.pdf
[58] Fitzpatrick R., 2012. Derivation of Von Karman Integral Formulation [Online] Available at: <http://farside.ph.utexas.edu/teaching/336L/Fluidhtml/node89.html> [Accessed 12 March 2014]
[59] Raspberry Pi Foundation, Raspberry Pi – Model B [computer], 2014.
[60] Meile, W., Brenn, G., Reppenhagen, A., Lechner, B. and Fuchs, A., 2011. Experiments and numerical simulations on the aerodynamics of the Ahmed body. *CFD Letters*, 3(1). pp.2-39.
[61] Douglas, J.F., Gasiorek, J.M. and Swaffield, J.A., 1979. *Fluid Mechanics*. London: Pitman Publishing.
[62] Baumers M, Tuck C, Bourell DL et al. Sustainability of additive manufacturing: measuring the energy consumption of the laser sintering process. IMechE Part B: J Eng Manuf 225:2228–2239